ACS Catalysis

Research Article

pubs.acs.org/acscatalysis

Direct Hydrogenation of Carbon Dioxide by an Artificial Reductase Obtained by Substituting Rhodium for Zinc in the Carbonic Anhydrase Catalytic Center. A Mechanistic Study

P. Piazzetta,[†] T. Marino,[*,†] N. Russo,[†] and D. R. Salahub[‡]

[†]Dipartimento di Chimica e Tecnologie Chimiche, Università della Calabria, 87036Rende, Italy

[‡]Department of Chemistry, IQST − Institute for Quantum Science and Technology, CMS − Centre for Molecular Simulation, BI 556, University of Calgary, 2500 University Drive NW, Calgary, Alberta Canada T2N 1N4

Supporting Information

ABSTRACT: Recently, a new artificial carbonic anhydrase enzyme in which the native zinc cation has been replaced with a Rh(I) has been proposed as a new reductase that is able to efficiently catalyze the hydrogenation of olefins. In this paper, we propose the possible use of this modified enzyme in the direct hydrogenation of carbon dioxide. In our theoretical investigation, we have considered different reaction mechanisms such as reductive elimination and σ-bond metathesis. In addition, the release of the formic acid and the restoring of the catalytic cycle have also been studied. Results show that the σ-bond metathesis potential energy surface lies below the reactant species. The rate-determining step is the release of the product with an energy barrier of 12.8 kcal mol^{-1}. On the basis of our results, we conclude that this artificial enzyme can efficiently catalyze the conversion of CO_2 to HCOOH by a direct hydrogenation reaction.

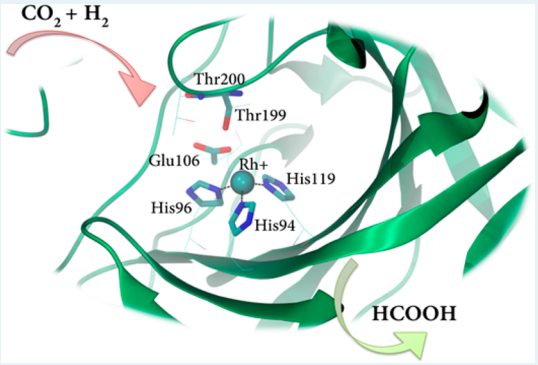

KEYWORDS: *DFT, Rh-carbonic anhydrase, carbon dioxide hydrogenation, biocatalysis, artificial enzyme*

INTRODUCTION

The increasing world energy demand makes imperative the search for alternative sources to fossil fuels. New chemical feedstocks must possess some characteristics that can be summarized in the following points: low cost and abundance; environmentally friendly; easily produced, stored, and transported. Although the use of hydrogen suffers from a series of unsolved problems such as security and storage, there is much evidence that indicates this source as a better candidate for the new "energy era" already called the Hydrogen Economy.[1−5] On the other hand, the enormous consumption of fossil fuels introduces into the atmosphere a huge amount of carbon dioxide that strongly contributes to global climate change[6] and is causing social and economic consequences. In this scenario, an ideal combination should be the concomitant use of H_2 and CO_2 for the production of energy and, simultaneously, the reduction of environmental pollution. Nontoxic, economic, and abundant carbon dioxide is thermodynamically stable, and its conversion into useful products is difficult and represents a challenge for modern chemical research.[7−15] In particular, its transformation into formic acid[16−19] can be considered as a valid means for hydrogen storage[20−22] because of its possible in situ consumption. The reduction of CO_2 to HCOOH can be done by a hydrogenation reaction by using efficient and specific catalysts. There are in the recent literature many examples of research devoted to this field,[23−28] but the proposed catalysts do not give catalytic turnover sufficient to justify their employment on an industrial scale. Nature can inspire new research because she uses extraordinary chemical machines, enzymes, that efficiently catalyze a huge number of reactions.

Very recently, a bacterial hydrogen-dependent carbon dioxide reductase from *Acetobacterium woodii* catalyzing the hydrogenation of CO_2, the hydrogen-dependent carbon dioxide reductase (HDCR), has been discovered and characterized.[29] In particular, this kind of enzyme makes physiological use of H_2 + CO_2 as the sole growth substrate and produces formate as an intermediate. This discovery opened a new frontier in biocatalysis, although the structure of the enzyme is not known and the reaction mechanism seems to involve different subunits, cofactors, and electron sources. Nature offers another well-studied class of enzymes, carbonic anhydrases, widely present in different organisms, that are able to transform CO_2 into carbonate[30−39] under physiological conditions but are not able to catalyze its direct hydrogenation. In a recent paper, Jing, Okrasa, and Kazlauskas[40] have demonstrated that the substitution of the natural zinc cation, in the active site of human CA, by a Rh(I) activates the reductase activity of this modified enzyme. In fact, the authors observe the stereo-

Received: January 29, 2015
Revised: August 3, 2015
Published: August 5, 2015

DOI: 10.1021/acscatal.5b00185
ACS Catal. 2015, 5, 5397−5409

Scheme 1. Proposed Pathway for Hydrogen Activation and CO_2 Insertion (path 1)

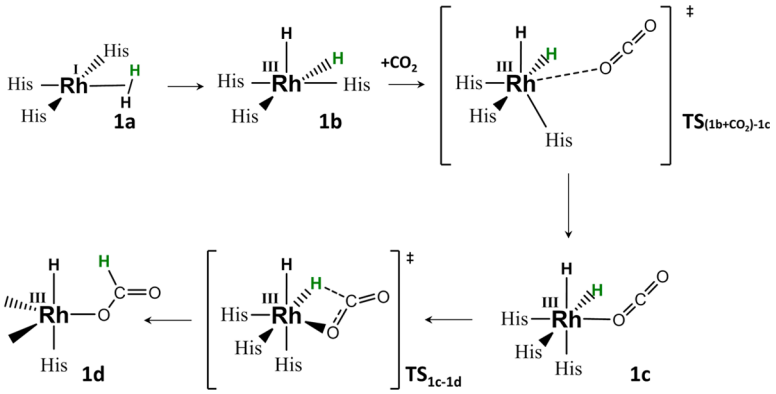

Scheme 2. Overview of the Investigated Formic Acid Formation Pathways Starting from 1d[a]

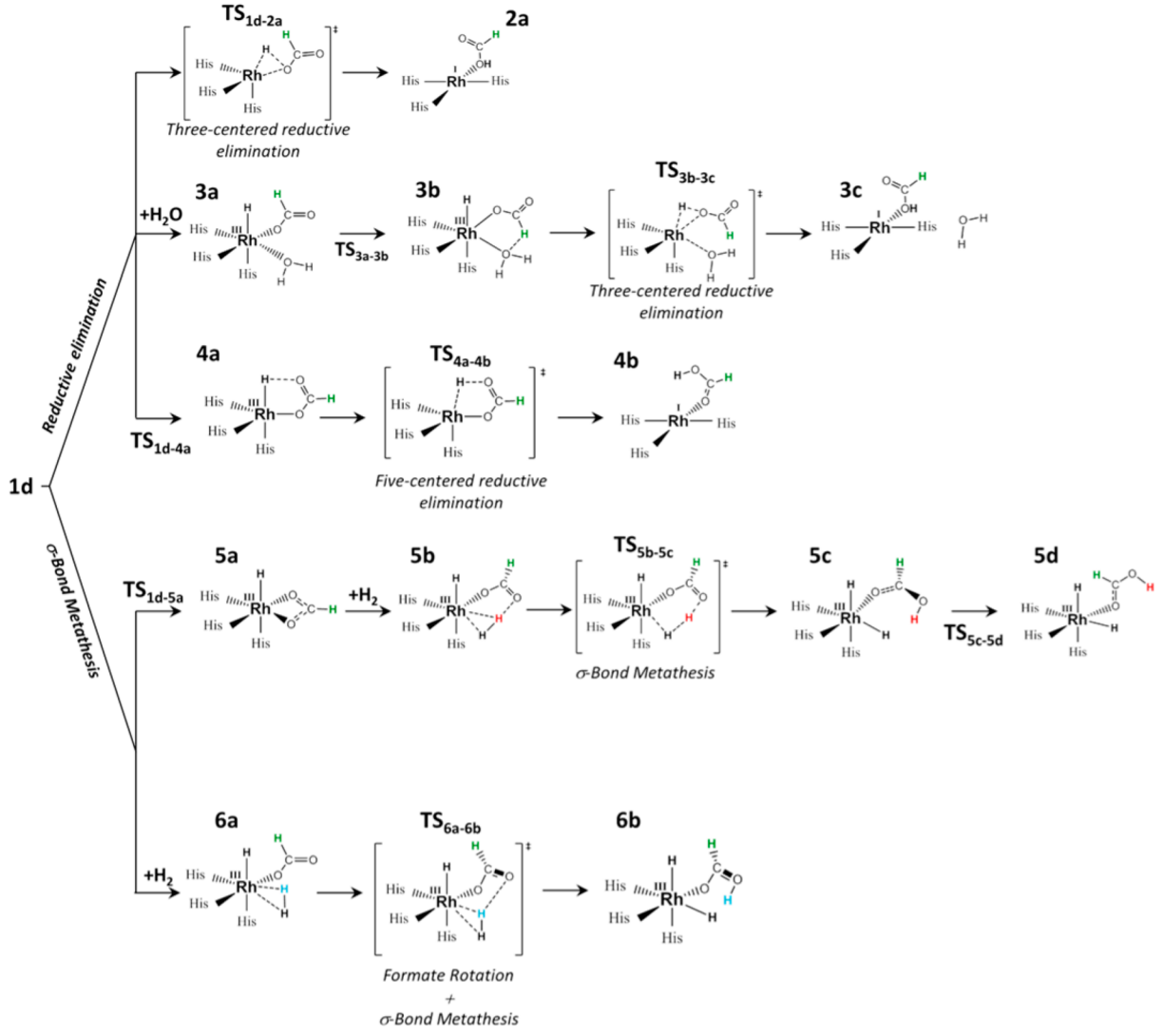

[a]Paths **2**, **3**, and **4** are related to reductive elimination and paths **5** and **6** to σ-bond metathesis and formate rotation, respectively.

selective direct hydrogenation of olefins with high catalytic efficiency.[40,41] Inspired by these recent and important discoveries, considering that some rhodium organometallic complexes have been previously proposed as promising catalysts for CO_2 hydrogenation[27,28,42,43] and continuing our previous work on the promiscuous ability of hCA,[44,45] we have

DOI: 10.1021/acscatal.5b00185
ACS Catal. 2015, 5, 5397−5409

undertaken a detailed theoretical work with the aim of verifying if the "artificial" Rh(I)-CA is able to efficiently catalyze the direct hydrogenation of carbon dioxide. Due to the novelty of these recent results and the lack of mechanistic information, different reaction mechanisms have been explored by using density functional theory and modeling the enzyme active site with a cluster model, in which, in addition to the primary ligands of the Rh(I), other amino acid residues that come into play in the catalytic process have been included.

COMPUTATIONAL METHODS

All the calculations have been performed at the DFT level of theory employing the B3LYP exchange-correlation functional,[46,47] as implemented in the Gaussian 03 program.[48] The geometry optimization has been carried out using the 6-31+G(d,p) basis set on all elements except for Rh, which has been described by the relativistic compact Stuttgart/Dresden effective core potential (SDD)[49] associated with its corresponding basis sets.

The final and the solvation energies have been calculated as single point corrections on the optimized structures using the PCM[50,51] continuum solvation model employing the larger 6-311+G(2d,2p) basis set for C, N, O, and H atoms and SDD for Rh and taking into account the dispersion contribution as suggested by Grimme et al.[52,53] (B3LYP-D3). The dielectric constant was chosen to be $\varepsilon = 4$, which is the most used value to represent the protein environment.[54−59]

In order to identify all the stationary points as minima (zero imaginary frequency) or transition states (one imaginary frequency) and to obtain ZPE corrections, analytic frequency calculations have been performed on all the optimized structures at the same level of theory used for the optimization step. We underline that, because some atoms were kept fixed at their X-ray crystallographic positions, this procedure gives rise to few small imaginary frequencies, typically on the order of 10*i* cm^{-1}. These frequencies do not contribute significantly to the ZPE and thus can be tolerated. The energies reported here are corrected for both solvation and zero-point vibrational effects.

The exact connection of that transition state with the two related minima has been checked by using the intrinsic reaction coordinate (IRC) computational procedure.[60,61]

NBO charge analysis[62] was carried out on the structures of some intercepted stationary points.

On the basis of previous studies on the H_2 and CO_2 activation on a series of complexes and considering the catalytic process of the native substrate of the hCAII, we have considered different reaction paths as depicted in Schemes 1 and 2. These paths include the hydrogen activation and subsequent CO_2 insertion (**path 1**), the formation of formic acid via reductive elimination (**paths 2**, **3**, and **4**) and σ-bond metathesis (**paths 5** and **6**). Lastly, we have also considered the restoring of the catalytic cycle by analyzing the releasing process of the formed product (**paths 4, 5, 6**).

Model. The model used to describe the reductase behavior of the Rh(I)-containing hCAII is depicted in Scheme 3. It has been obtained from the crystallographic structure (PDB = 2CBA) where the native zinc ion has been replaced by Rh(I). The obtained cluster mimicking the active site of the enzyme contains a Rh(I) coordinated to the imidazoyl nitrogen atoms modeling the three histidine residues (His94, His96, His119) as primary ligands. The tetracoordination of Rh(I) is then reached by adding a water molecule occupying the fourth position around the metal ion. Furthermore, three indirect ligands of the metal center represented by truncated models of the Glu106, Thr199, and Thr200 complete the model (50 atoms, charge = 0). The presence of these amino acid residues is believed crucial in the approach of CO_2 and the release of HCOOH due to the formation of an extended H-bond network. The atoms where the truncation has been made, have been kept frozen at their X-ray crystal positions during the optimization procedure, to preserve the spatial arrangement of the residues. These centers are indicated by stars in Scheme 3. This cluster model was found to be adequate in the elucidation of the catalytic mechanism followed by hCAII toward native CO_2[63−65] and other isoelectronic promiscuous substrates studied in previous works.[44,45] In particular, we mention that the computed barrier for the CO_2 substrate is about 2 kcal mol^{-1} different from that extracted from an experimental kinetics study.[44]

Scheme 3. Selected Model of the hCAII Active Site[a]

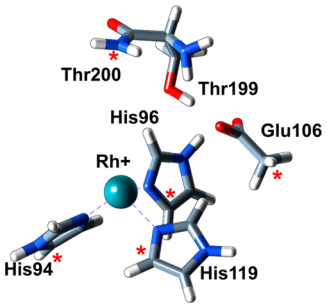

[a]Stars indicate the atoms that are fixed to their X-ray positions (PDB = 2CBA).

RESULTS AND DISCUSSION

Oxidative Addition and CO_2 Insertion. The first step of the [Rh(hCAII)] activation (see Scheme 1) concerns the substitution of the coordinated water molecule at the metal center Rh(I) with an H_2 molecule and occurs with a destabilization energy of 4.5 kcal mol^{-1} (**1a**). The species formed can undergo oxidative addition with the formation of the **1b** product. All the attempts to find a transition state for this H_2 bond activation failed. As a consequence, the geometry changes from a square planar to a square pyramidal geometry with an apical hydride due to the presence of σ donor ligands (His94, His96, His119) in a d^6 transition metal complex.[66] Enlarging the cluster by adding other closer residues (Tyr7, Asn62, His64, Asn67, Gln92, His107, Glu117, Val121, Val143, Leu198, Val207, Trp209, Asn244, Arg246), in the framework of a QM/QM′ method (see Supporting Information section), we obtained similar results for both the energetic and structural behaviors (see Figure S1). A further comparison between our QM model with the structure of **1a** obtained by the minimization at the QM/MM level of the entire protein reveals a similar geometrical behavior in the coordination region of the metal, as shown in Figure S1.

The barrierless oxidative H_2 addition is not unusual and has been found in previous studies[66,72] where, as in our case, the metal center is coordinated to strong sigma donor ligands. One of the referees suggests to consider heterolytic H_2 activation with the assistance of the Glu106 residue. We have explored this alternative path, and it turns out to be less probable because of the presence of Rh(I) species that requires tetracoordination and a long H_2−Glu106 distance (3.906 Å). Furthermore, due to the involvement of Glu106 in an H-bond

DOI: 10.1021/acscatal.5b00185
ACS Catal. 2015, 5, 5397−5409

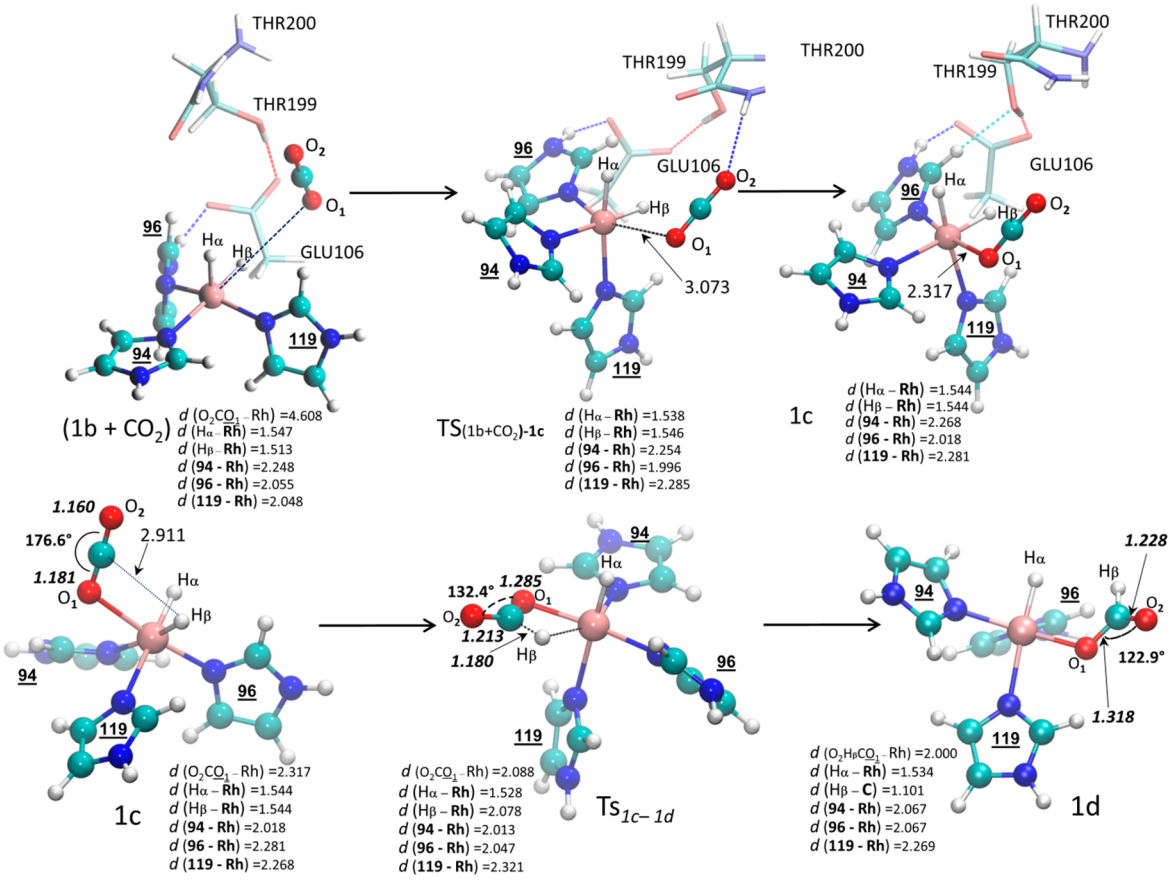

Figure 1. DFT optimized geometrical structures for all the species intercepted through the hydrogen activation and CO_2 insertion (**path 1**) with selected structural parameters (distances in Å). In **1c**, $\mathbf{TS_{1c-1d}}$, and **1d** species, the Glu106-Thr200-Thr199 triad is omitted for clarity. The d(94-Rh), d(96-Rh), and d(119-Rh) labels refer to the distances between the Rh and the coordinated nitrogens of His96, His94, and His119.

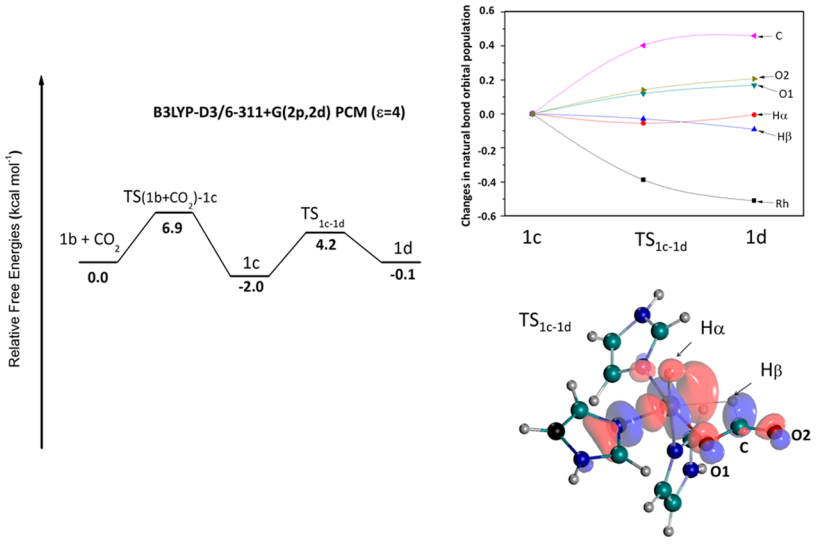

Figure 2. Calculated B3LYP-D3 free-energy profile for the hydrogen activation and CO_2 insertion (**path 1**). Energies (kcal mol^{-1}) are relative to the asymptote of the reactants. Population changes occurring in **path 1**. A positive value represents an increase in population relative to the 1c species. HOMO contour plot in the $\mathbf{TS_{1c-1d}}$ species.

interaction with Thr199, this residue becomes a poor proton acceptor. In addition, we have explored a possible mechanism maintaining the original square planar geometry of the Rh(I) complex and involving a water molecule as a proton shuttle between the hydrogen and Glu106. This path requires a higher energy (15.2 kcal mol^{-1}, see Figure S2) than the oxidative addition transition state. Turning to discuss our PES, we show the exothermicity of the step with the **1b** product that lies at 2.1 kcal mol^{-1} below **1a**. These findings confirm that Rh is an effective metal in H_2 oxidative addition.[67]

CO_2 insertion into the Rh(III) – H bond of [cis-RhH_2(hCAII)] starts with the formation of an octahedral

DOI: 10.1021/acscatal.5b00185
ACS Catal. 2015, 5, 5397–5409

precursor complex (**1b+CO$_2$**) where the CO_2 is placed at a distance of 4.608 Å from the metallic center (see Figure 1). This behavior is different from that found in the case of cis-$[Rh(III)H_2(PH_3)_3]^+$ and cis-$[Rh(III)H_2(PH_3)_2(H_2O)]^+$ catalyst models that did present a CO_2 directly coordinated to the rhodium center (2.464 and 2.320 Å, respectively).[42] In the enzyme the presence of the Glu106-Thr199-Thr200 triad, retained in our model, does allow the formation of a stable complex (**1b+CO$_2$**). The formation of the coordinated intermediate (**1c**) requires an activation barrier of 6.9 kcal mol^{-1} (see Figure 2). In the transition state (**TS$_{1b+CO2-1c}$**) CO_2 establishes, by the O atom, a weak interaction with the NH_2 moiety of Thr199 and is located at 3.073 Å from the rhodium center (see Figure 2). In order to accommodate the incoming CO_2, the His119 ligand is involved in a gradual migration from the equatorial position to the axial one with an increment in Rh−His119 distance of 0.233 Å due to the trans effect of H_α.[68] Also in this case, the structure of **TS$_{1b+CO2-1c}$** arising from the application of the QM/QM′ method and displayed in comparison with the QM one in Figure S3 shows that the octahedral geometry is preserved.

The structure of this transition state shows that the CO_2 acts as a Lewis base coordinating through one oxygen atom, as normally occurs at electron−deficient metal centers.[69] The **1c** complex formed turns out to be more stable than **1b+CO$_2$** by 2.0 kcal mol^{-1}. From **1c** CO_2 is inserted into the Rh(III) − H bond by a four-centered TS (**TS$_{1c-1d}$**) giving rise to the **1d** species in which the OCOH fragment is coordinated to the rhodium center in an η^1 fashion. The imaginary frequency in **TS$_{1c-1d}$** (60.1i cm^{-1}) mainly involves Rh−H_β bond breaking and C−H_β bond formation. The geometrical features of this transition state indicate that the η^1-formate anion is almost formed. This can be seen also by the HOMO contour plot shown in Figure 2. The **1d** complex is characterized by a five-coordinated pseudo square-pyramidal geometry (see Figure 1) and lies at only 0.1 kcal mol^{-1} below the reactant energies.

The NBO population of the C atom increases as the insertion proceeds, while that of the Rh decreases. This behavior (see Figure 2) clearly indicates that a charge transfer from Rh to CO_2 occurs during the η_1-formate formation. The net charges at the TS are almost the same as that of the product, confirming that the formate anion is almost formed. H_α and H_β population remains substantially unchanged during the reaction, allowing the hypothesis that both the charge transfers from H_β to C and from Rh to H_β participate in the CO_2 activation.

Reductive Elimination (Path 2, 3, 4). As depicted in Scheme 2, the reductive elimination of the η^1-formic acid can occur following two different paths characterized by the formation of three-centered (**paths 2, 3**) and five-centered (**path 4**) transition states.

The computed potential energy surfaces for the **paths 2** and **4** are reported in Figure 3, whereas the optimized geometries of all the species related to **paths 2**, **3**, and **4** are shown in Figure 4.

Starting from **1d**, in **path 2**, the proton transfer of the apical Hα atom moves toward the O1 atom (without a filling of the geometrical vacancy of the pseudo square pyramidal structure), giving rise to the three-centered **TS$_{1d-2a}$** characterized by an imaginary frequency (1030.8i cm^{-1}) whose eigenvector involves the Hα shifting to O_1. This TS lies at 20.8 kcal mol^{-1}, and the final product (**2a**), in which the formic acid is coordinated to the Rh cation through the OH group, is

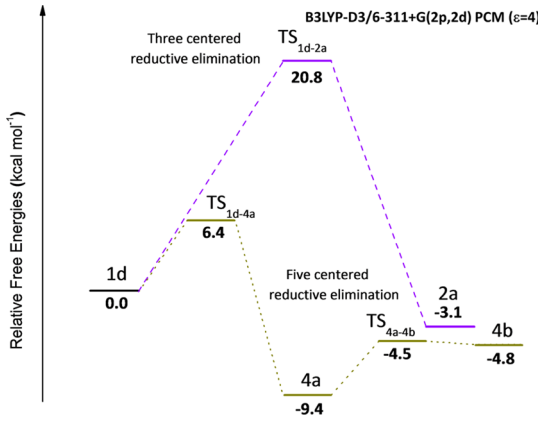

Figure 3. Calculated B3LYP-D3 free energy profiles for the three-centered path (**2**) and five-centered path (**4**) reductive elimination. Energies (kcal mol^{-1}) are relative to the asymptote of the reactant (**1d**).

exothermic by 3.1 kcal mol^{-1} with respect to the **1d** starting species. The IRC picture of this step is reported in Figure S4. The **2a** product takes a four-coordinated planar structure (Figure 4) due to the d^8 electron configuration of Rh(I) and the Rh−O_1 distance (2.255 Å) is longer than the corresponding distance in the **1d** formate adduct. Following this path (Figure 3), the formation of formic acid requires a relatively high energy barrier (20.8 kcal mol^{-1}). A similar behavior (with an activation energy of 19.6 kcal mol^{-1}) has been previously found in the case of CO_2 reductive elimination catalyzed by a Wilkinson-like complex.[47]

Due to the presence of this higher energy barrier, we have considered the possibility that in this process a water molecule, that could fill the vacancy in the **1d** structure, can assist the formic acid formation (**path 3** in Figure 5). In this situation, the first step of the reaction is the formation without an energy barrier of a monohydrate octahedral complex **3a** (see Scheme 2 and Figure 4) with a stabilization energy of 19.5 kcal mol^{-1} with respect to **1d** (Figure 5). In this complex, the water is coordinated to the Rh with a distance of 2.046 Å, and the rhodium coordination geometry is now octahedral. The subsequent isomerization (**3a** → **3b**) occurs with a rotation along the O_1−C bond and the relative transition state (**TS$_{3b-3c}$**) lies at only 0.7 kcal mol^{-1} above the reactants. The resulting intermediate (**3b**) is very stable (−30.8 kcal mol^{-1}) and is characterized by a hydrogen bond between the formate oxygen and one hydrogen of the water molecule (1.510 Å). From this point an energetically prevented three-centered TS (**TS$_{3b-3c}$**) at 42.2 kcal mol^{-1} involves the Hα shifting toward O_1, with the concomitant expulsion of the water molecule from the rhodium coordination sphere (**3c**) (see Figure 5). From these results, it is evident that, also in the presence of a water molecule the three- centered transition state reductive elimination requires high energies. In going from **3b** to **3c** intermediate, in principle, a five-centered transition state can be hypothesized. Our results concerning the location of this TS show that during the relaxed energetic scan procedure, His119 is expelled from the inner coordination shell (see Figure S5).

As shown in Scheme 2, an alternative path is the five-centered reductive elimination. The potential energy profile for this process is reported in Figure 3, whereas the geometries of the species characterizing this path are depicted in Figure 4. The initial step is the isomerization of **1d** to **4a** that occurs with

DOI: 10.1021/acscatal.5b00185
ACS Catal. 2015, 5, 5397−5409

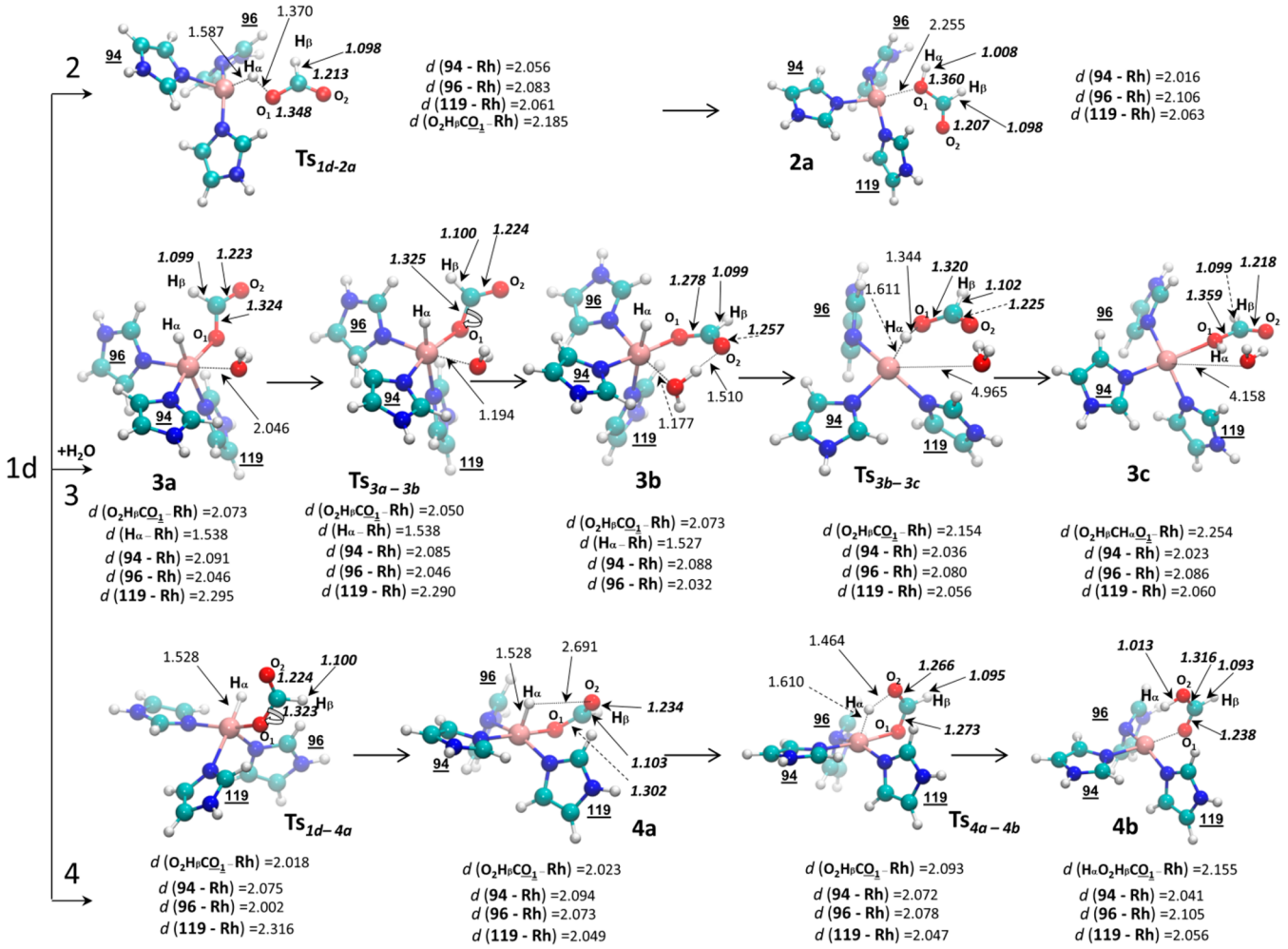

Figure 4. DFT optimized geometrical structures for all the species intercepted through paths **2**, **3**, and **4** with selected structural parameters (distances in Å). The Glu106-Thr200-Thr199 triad is omitted for clarity. The d(94-Rh), d(96-Rh), and d(119-Rh) labels refer to the distances between the Rh and the coordinated nitrogens of His96, His94, and His119.

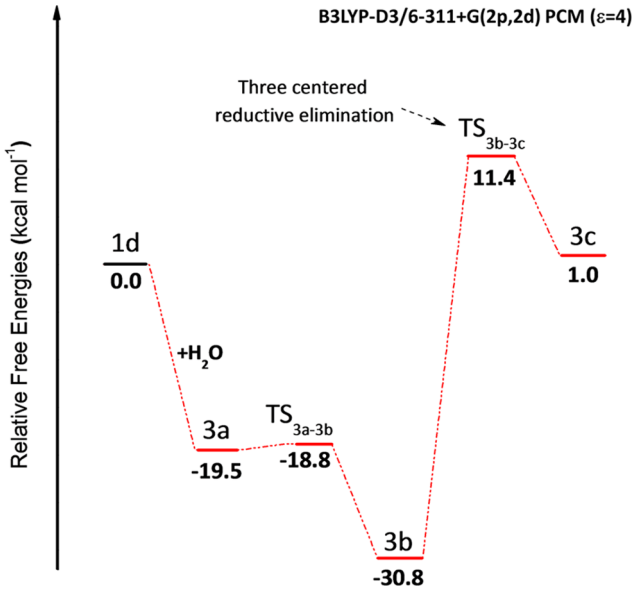

Figure 5. Calculated B3LYP-D3 free-energy profile for the three-centered path (**3**) reductive elimination assisted by water. Energies (kcal mol^{-1}) are relative to the asymptote of the reactant (**1d**).

a rotation around the O_2–C bond. This topological change is necessary to prearrange the formate in a fashion suitable to form a five-centered interaction with the Rh–H moiety. The located **TS$_{1d-4a}$** (176.1*i* cm^{-1}) has a rearrangement of geometry, that remains a square planar pyramid, involving His119 that moves on the plane formed by His94, His96, and η^1-formate. The related energy is calculated to be 6.4 kcal mol^{-1} above **1d** (see Figure 3). The five-centered reductive elimination occurs through **TS4a–4b** (526.9*i* cm^{-1}) with an activation energy of only 4.9 kcal mol^{-1}. The structure of this transition state indicates that the Rh–Hα bond is practically broken (1.610 Å), whereas the value of the O_2–Hα distance (1.464 Å) suggests the initial bond formation (see Figure 4). The IRC relative to this step is reported in Figure S6.

The analysis of the NBO behaviors for the considered reductive elimination paths are reported in Figure 6. As shown in this Figure, the Hα atomic population decreases in both reductive eliminations because Hα mutates into a proton. The differences in terms of activation energies between the two mechanisms can be related to the fact that in the three-centered reductive elimination paths (**2** and **3**), the p orbital of the O_1 atom must change its direction toward Hα. Such a direction change suppresses the charge transfer from the formate to the Rh, on the other hand, the O_2 p orbital in the five-centered

DOI: 10.1021/acscatal.5b00185
ACS Catal. 2015, 5, 5397–5409

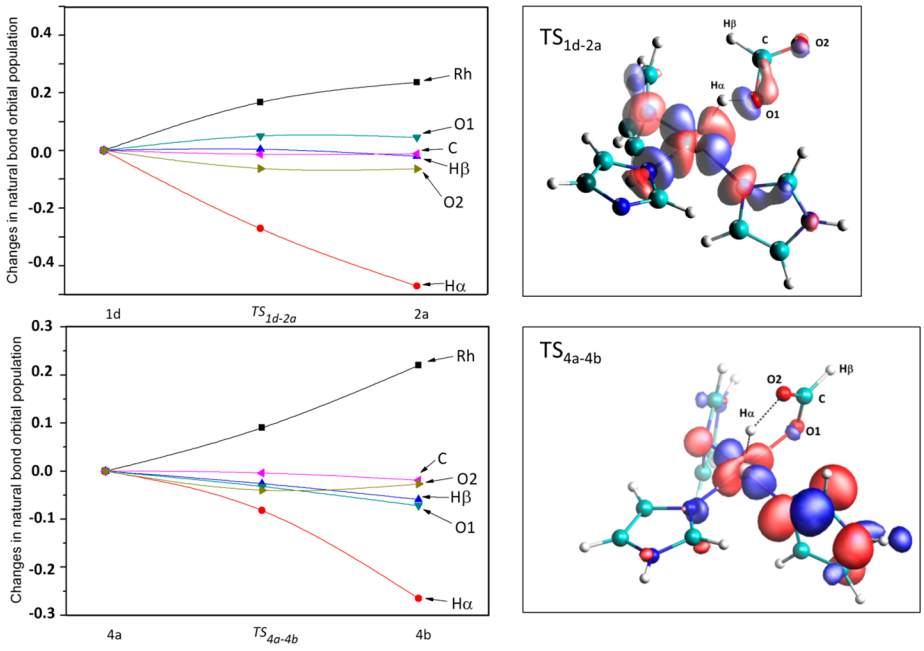

Figure 6. Changes in natural atomic orbital population occurring in **paths 2** and **4.** A positive value represents an increase in population relative to **1d** (**path 2**) and **4a** (**path 4**) species. HOMO contour plots are related to the $\mathbf{TS_{1d-2a}}$ and $\mathbf{TS_{4a-4b}}$ species. Absolute natural charge values for Rh in both paths are **1d** 0.389 lel, $\mathbf{TS_{1d-2a}}$ 0.222 lel, **2a** 0.153 lel and **4a** 0.281 lel, $\mathbf{TS_{4a-4b}}$ 0.191 lel, **4b** 0.061 lel.

reductive elimination is well oriented and expands toward Hα while the O_1 population decreases with the elongation of the Rh−O_1 bond (see Figure 6). Furthermore, the five-membered path suffers from a minor strain with respect to the three-membered one, and consequently, the formation of this geometry is more favorable.

We conclude that the reductive elimination path of **1d** that occurs through the formation of a five-centered transition state ($\mathbf{TS_{4a-4b}}$) is the favored one.

***σ*-Bond Metathesis (Paths 5, 6).** Other than reductive elimination, we have considered also the possibility that the enzymatic production of formic acid can follow other paths in which a σ-bond metathesis should be the main mechanism (see Figure 7). In this hypothesis, two distinct paths have been considered (see Scheme 2). In the first path (**path 5**), the formate that is monocoordinated to the Rh cation (**1d**) undergoes a rotation forming an η^2-formate product coordinated to Rh in a bidentate way (**5a**). This step can be understood because the Rh(III) ion tends to form a six-coordinated complex due to its d^6 electron configuration. The transition state connecting these two minima ($\mathbf{TS_{1d-5a}}$) requires 3.7 kcal mol^{-1} with respect to the asymptotic limit (see Figure 7) and occurs through a rotation of the −OCOH moiety. The value of the imaginary frequency (159.2*i* cm^{-1}) accounts well for this movement. The O−Rh distances are now 2.128 and 2.136 Å, showing the bidentate nature of the Rh(III) formate interaction (see Figure 8). The product **5a** is 12.3 kcal mol^{-1} more stable than **1d** and the system assumes an octahedron-like geometry in which the O_1−Rh−NHis96 angle is 102.2° and His96 is in a staggered plane with respect to the plane formed by the other equatorial ligands. This arrangement allows the insertion of a new H_2 molecule on the same side of the O_1 atom of [RhH(η^2−O_2CHO_1(hCAII)]. The formed species **5b** is 3.8 kcal/mol more stable than **5a** and the insertion of the molecular hydrogen breaks the formate bicoordination (see Figure 8). From this intermediate, the σ-bond metathesis takes place via a six-centered TS ($\mathbf{TS_{5b-5c}}$) with a negligible activation energy (0.9 kcal mol^{-1}) (see also the relative IRC reported in Figure S7). The analysis of the related imaginary frequency (473.6*i* cm^{-1}) clearly shows that the H−Rh bond is being formed and the hydrogen transfer to the oxygen is in progress (H_1−O_1 distance is 1.453 Å). We underline that the PES region describing the σ-bond metathesis process appears flat enough that the reaction proceeds without a barrier for the formation of the formic acid-containing complex (**5c**) that is stabilized by 20.0 kcal mol^{-1} (Figure 7). No significant geometrical changes occur during the process, apart from the elongation of the Rh−His94 distance due to the trans effect of H_2. As shown in Figure 9, the H_1 atomic population decreases in the σ-bond metathesis because H_1 takes a favorable position to form an interaction with the O_1 p orbital of the HOMO. The

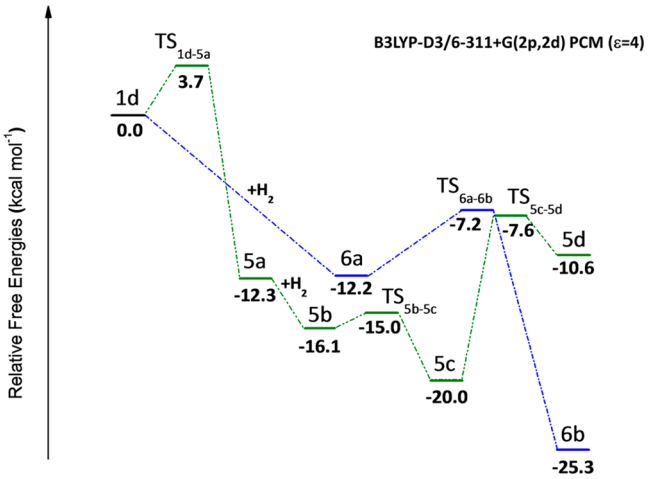

Figure 7. Calculated B3LYP-D3 free energy profiles for the σ-bond metathesis explored pathways (**5** and **6**). Energies (kcal mol^{-1}) are relative to the asymptote of the reactant (**1d**).

DOI: 10.1021/acscatal.5b00185
ACS Catal. 2015, 5, 5397−5409

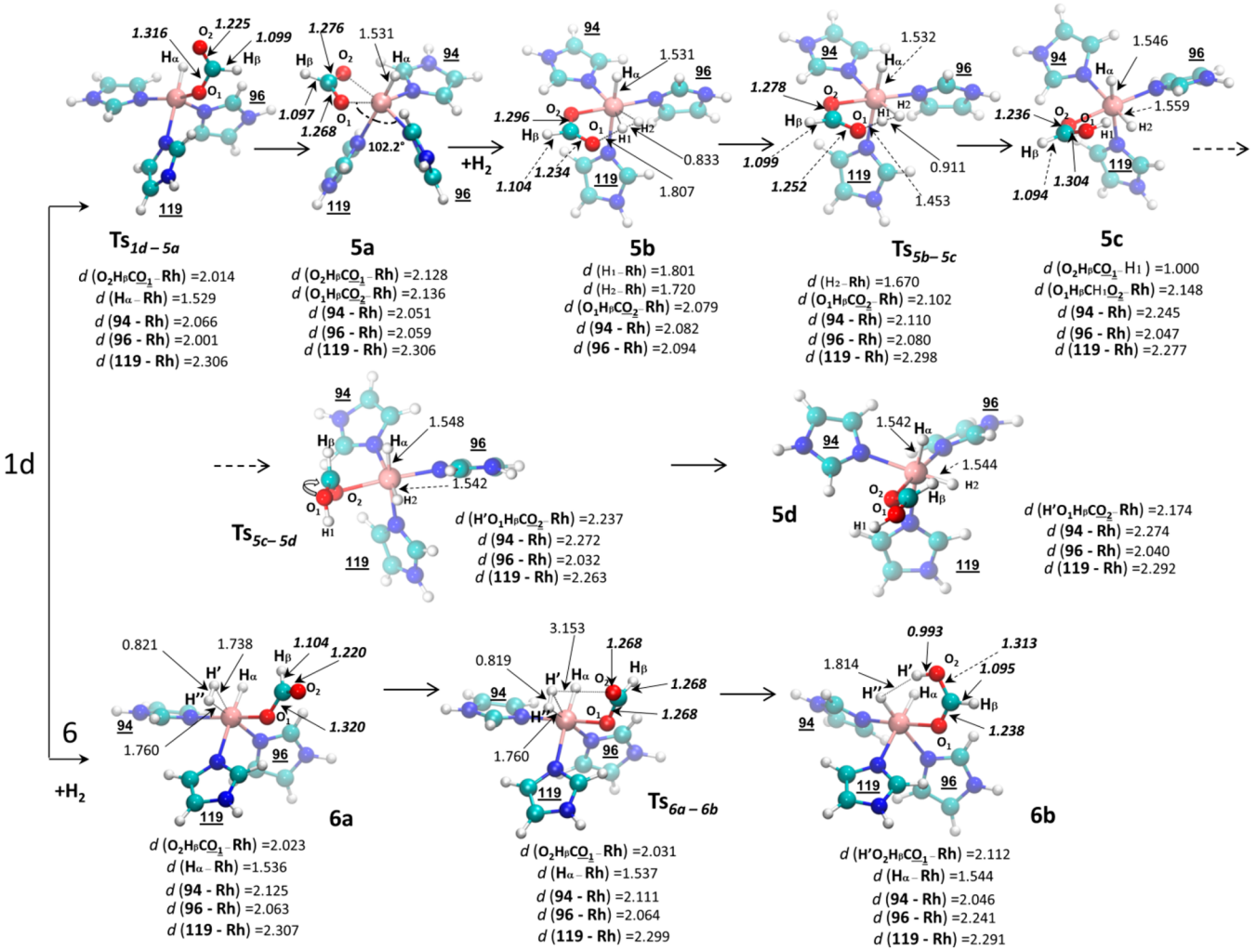

Figure 8. DFT optimized geometrical structures for all the species intercepted through paths **5** and **6** with selected structural parameters (distances in Å). The Glu106−Thr200−Thr199 triad is omitted for clarity. The d(94-Rh), d(96-Rh), and d(119-Rh) labels refer to the distances between the Rh and the coordinated nitrogens of His96, His94, and His119.

lone pair on the oxygen atom is oriented toward the incoming hydrogen and acts as a trigger in the H_1-H_2 heterolytic cleavage. Moreover, the η_1-formic acid product (**5c**) can isomerize through a rotation of the $Rh-O_2-C-H_\beta$ dihedral leading to the formation of a less stable isomer by 9.4 kcal mol^{-1} (**5d**). This isomerization occurs through a transition state ($\mathbf{TS_{5c-5d}}$) with an activation energy of 12.4 kcal mol^{-1} (Figure 7).

The other explored path includes a rotation of the formate (**path 6** of Figure 7). In this alternative way, the molecular hydrogen is directly linked into the **1d** intermediate, filling the vacancy in this species with the formation of an octahedral complex (**6a**) lying at 12.2 kcal mol^{-1} below **1d**. The reaction proceeds directly with the formation of a complex, in which the formic acid is linked to the Rh(III) (**6b**), with an activation energy of only 5 kcal mol^{-1}. The process is characterized by the rotation of the $\eta 1$−formate with the concomitant formation of a concerted σ-bond metathesis $\mathbf{TS_{6a-6b}}$. (see Figure 8). The imaginary frequency of 171.2*i* cm^{-1} is related to rotational modes and both $Rh-O_1$ and $C-O_2$ stretches. The topology of $\mathbf{TS_{6a-6b}}$ is different from the corresponding transition state in **path 5**. The low energy barrier associated with this TS (see Figure S8 for the relative IRC) can be elucidated by analyzing the MO representation and the NBO population (see Figure 9). During the formate rotation, a lone pair of the O_2 atom orients itself to establish a positive overlap with the H′ atom. Compared to **path 5**, both Rh and O_1 populations decrease slightly following the formate moiety rotation. We can conclude that during this dualistic process a new hybridization occurs and allows the best overlap between H′ and O_2 with the formation of a covalent interaction. Furthermore, as suggested by one of the referees, we have explored a pathway in going from **3b** to **6a**. The activation energy for this process is 35.5 kcal mol^{-1} (Figure S9), meaning that this alternative mechanism is unfavorable.

Release of the Formic Acid and Restoring of the Catalytic Cycle. In both enzymatic and nonenzymatic reactions, the restoring of the catalytic cycle can be the rate-determining step.[70−72] In our case, the release of the formic acid product should be a crucial point in restoring the catalyst. Kinetic and theoretical investigations demonstrate how the presence of a base can facilitate the liberation of formic acid.[72] This aspect has been confirmed in the case of Ru complexes in which a Lewis base is necessary to release formic acid.[73]

For this reason, we have also explored this process (Scheme 4), considering the addition of a hydrogen or a carbon dioxide molecule necessary to restore the catalytic cycle by removing the formic acid produced at the end of **paths 4**, **5**, and **6** (see

DOI: 10.1021/acscatal.5b00185
ACS Catal. 2015, 5, 5397−5409

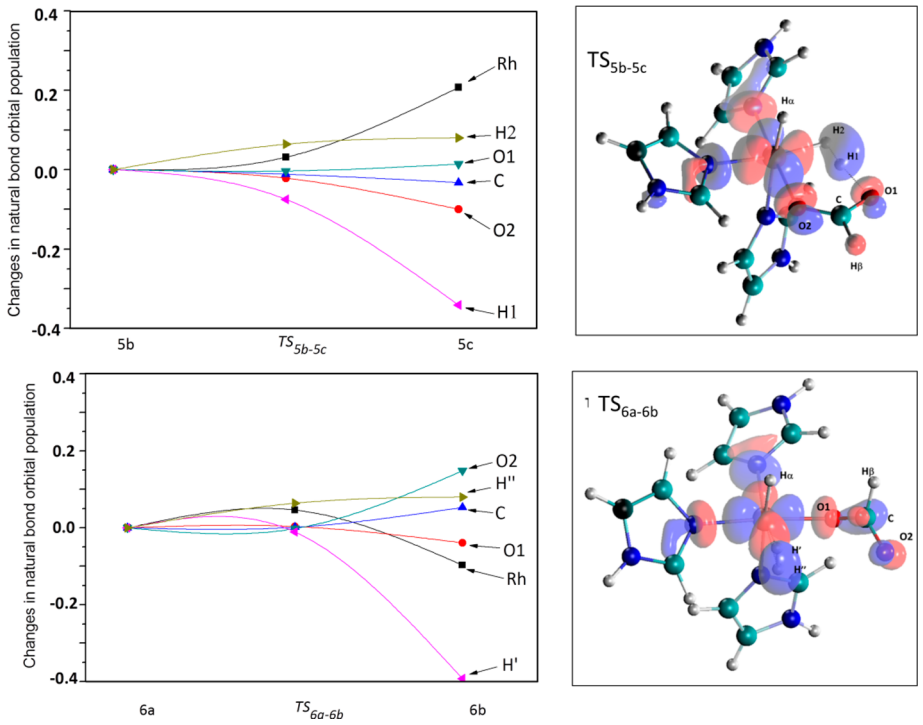

Figure 9. Changes in natural atomic orbital population occurring in path **5** and **6**. A positive value represents an increase in population relative to **5b** (path **5**) and **6a** (path **6**) species. HOMO contour plots are related to the $\mathbf{TS_{5b-5c}}$ and $\mathbf{TS_{6a-6b}}$ species. Absolute natural charge values for Rh in both paths are **5b** 0.045 lel, $\mathbf{TS_{5b-5c}}$ 0.014 lel, **5c** −0.162 lel and **6a** 0.031 lel, $\mathbf{TS_{6a-6b}}$ 0.032 lel, **6b** −0.160 lel.

Scheme 4. Overview of the Explored Formic Acid Release Pathways from path 4 (Reductive Elimination) and paths 5 and 6 (σ-Bond Metathesis and Formate Rotation, Respectively)

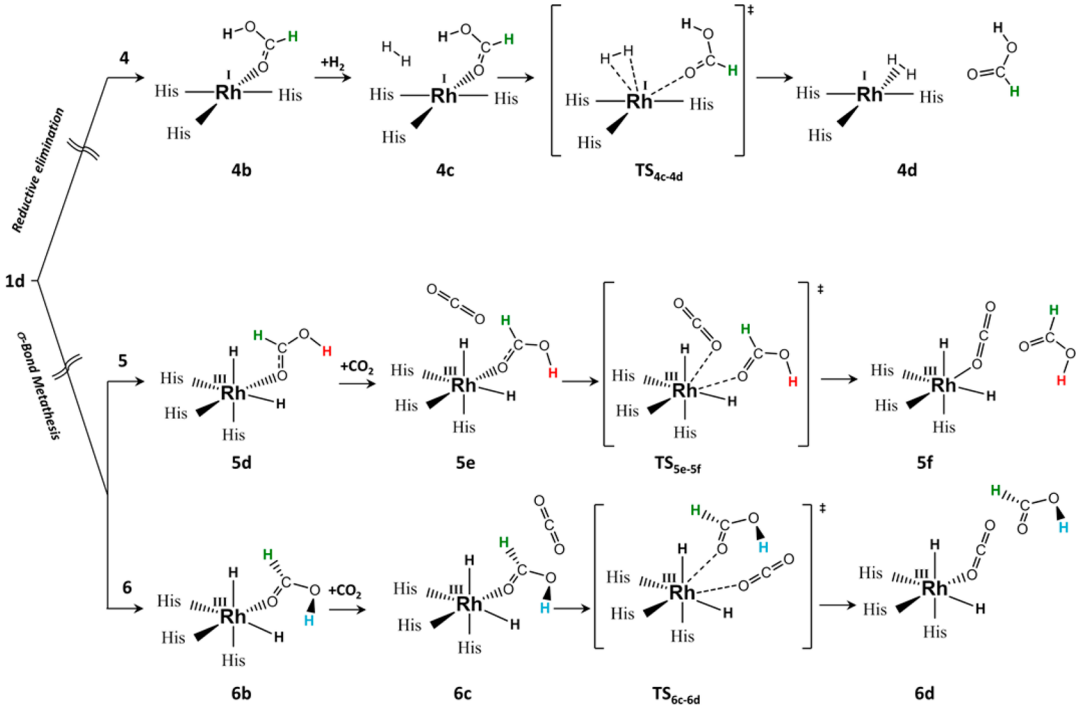

Figure 10 and Scheme 4). The related optimized species are shown in Figure 11. The final product of reductive elimination (**path 4**) is the species **4b**; therefore, an entering H_2 ($H_3 - H_4$) can give rise to the formation of **1a** and the detachment from the Rh center of the formic acid. As shown in Figure 10, the potential energy surface for this process includes the formation of a new intermediate **4c**, in which H_2 interacts weakly with the Rh cation (see Figure 11) and its energy lies at only 1.9 kcal mol^{-1} above **4b**. The subsequent insertion of molecular hydrogen in the Rh coordination sphere requires a barrier of 10 kcal mol^{-1} to be overcome and occurs through the transition state ($\mathbf{TS_{4c-4d}}$). The imaginary frequency (307*i* cm^{-1}) clearly

DOI: 10.1021/acscatal.5b00185
ACS Catal. 2015, 5, 5397−5409

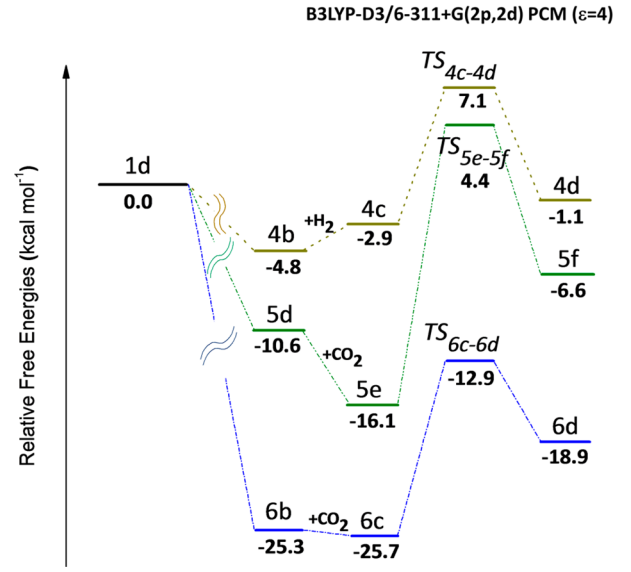

Figure 10. Calculated B3LYP-D3 free energy profiles for formic acid release explored pathways. Energies (kcal mol^{-1}) are relative to the asymptote of the reactant (**1d**).

indicates the H_2 insertion step. In the final product **4d**, which is stabilized by only 1.1 kcal mol^{-1} with respect to **1d**, the H−Rh distances are 1.662 and 1.670 Å, the H_3−H_4 distance is 0.881 Å, and the formic acid is detached from the Rh center (4.492 Å). As shown in Figure 11 the Thr200 residue seems to help the release of the formic acid.

The restoring of the catalyst starting from the products obtained from σ-bond metathesis mechanisms (**paths 5** and **6**) requires the interaction with a new carbon dioxide molecule. According to what happens in the CO_2 insertion, where CO_2 acts as a Lewis base coordinating the metal center through one oxygen atom, we investigated the release of the formic acid from both **5d** and **6b** complexes. In the first adduct, for both the paths, the CO_2 is linked to the complex by weak interactions with consequent slight energy stabilization. Both the starting complexes have octahedral coordination and the insertion is more difficult. In fact the located transition states, $\mathbf{TS_{5e-5f}}$ and $\mathbf{TS_{6c-6d}}$, impose barriers of 20.5 and 12.8 kcal mol^{-1}, respectively (see Figure 10). The lowest energy barrier for the $\mathbf{TS_{6c-6d}}$ is also due to the presence of an H-bond between the OH moiety of formic acid and the corresponding group of Thr199 (1.564 Å, see Figure 11). This hydrogen bond is retained in the **6d** species (1.586 Å) that turns out again to

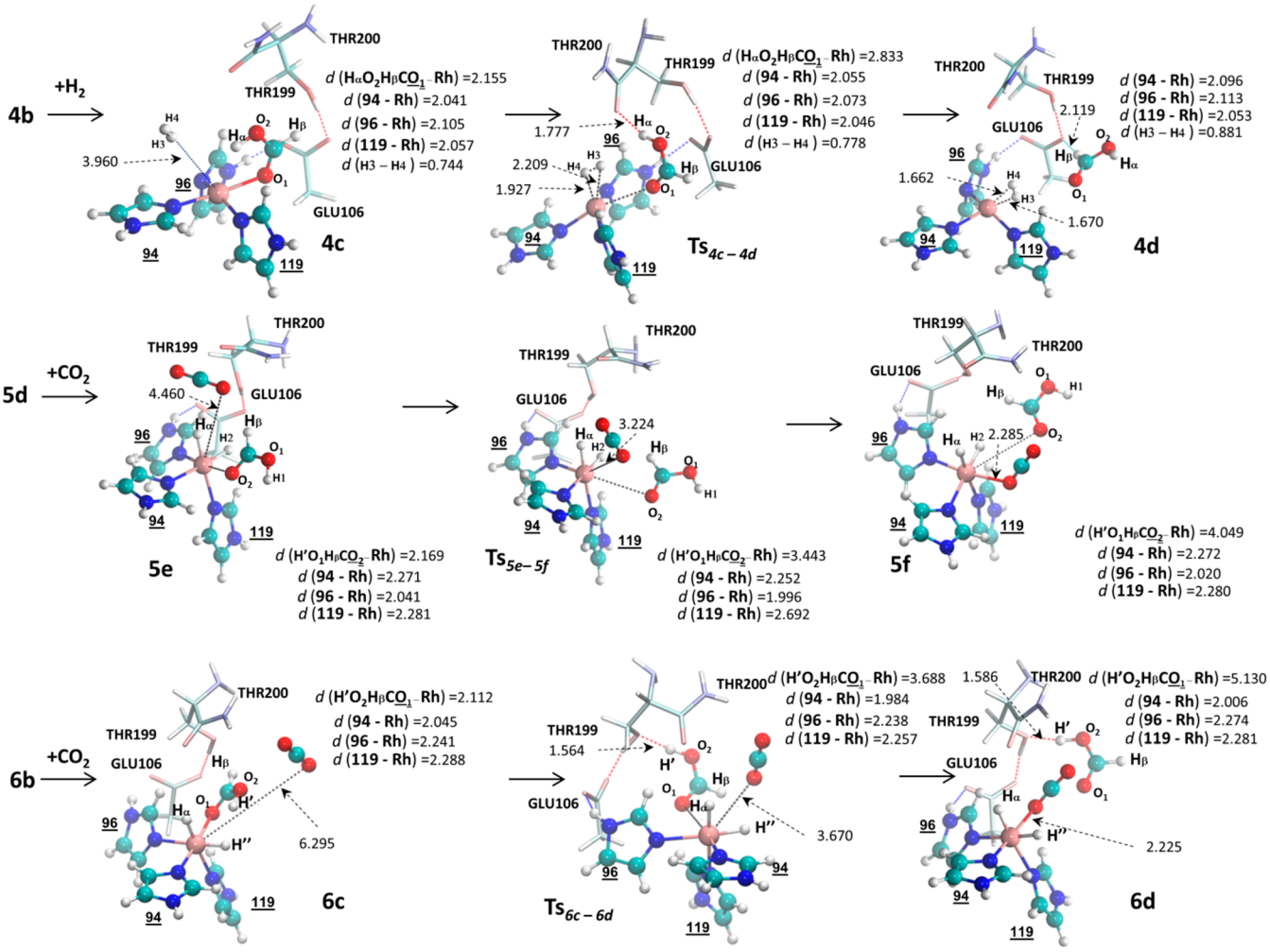

Figure 11. DFT optimized geometrical structures for all the species intercepted through the explored paths for formic acid release starting from **4d**, **5b**, and **6b** species with selected structural parameters (distances in Å). The Glu106−Thr200−Thr199 triad is retained. The d(94-Rh), d(96-Rh), and d(119-Rh) labels refer to the distances between the Rh and the coordinated nitrogens of His96, His94, and His119.

DOI: 10.1021/acscatal.5b00185
ACS Catal. 2015, 5, 5397−5409

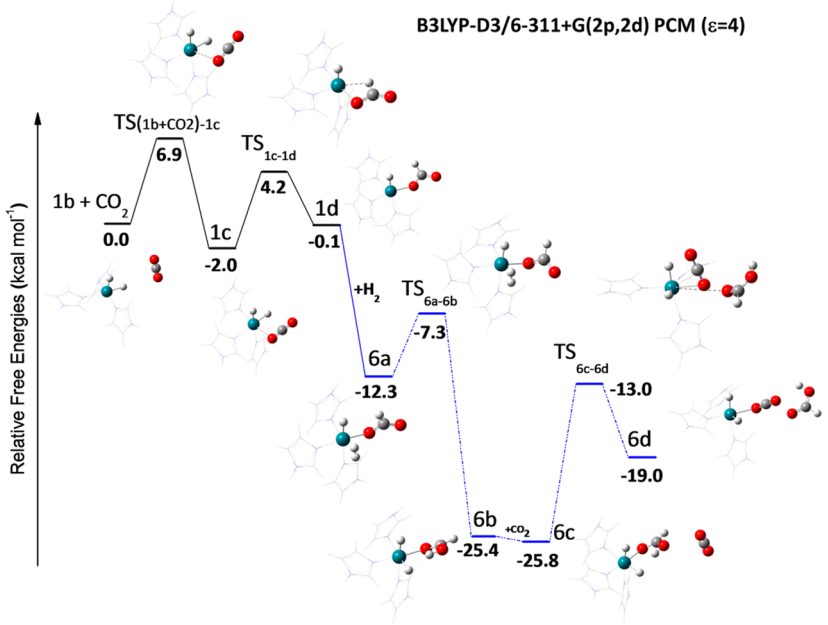

Figure 12. Calculated B3LYP-D3 free energy profile for the best mechanism arising from the present investigation. Energies are in kcal mol^{-1}.

be more stable than **5f**. In both final complexes, the carbon dioxide is coordinated to the Rh center (Rh−O distances of 2.285 and 2.225 Å for **5f** and **6d**, respectively), although the formic acid is clearly released (Rh−O distances of 4.049 and 5.130 Å for **5f** and **6d** respectively).

From the data reported in Figure 10, we underline that both **paths 4** and **5** show transition-state energies that lie above the asymptotic limit (**1d** energy); however, the whole species intercepted along the **path 6** lie below **1d**. This means that we can propose **path 6** as the preferred one for the restoring of the catalytic cycle.

The entire potential energy surface for the preferred reaction path is summarized in Figure 12.

CONCLUSIONS

Motivated by the recent experimental evidence that a modified carbonic anhydrase, in which the native zinc cation is substituted with a Rh(I) center, is able to act as a reductase enzyme able to efficiently catalyze the hydrogenation of olefins, we have explored at the DFT level of theory, the possibility that the carbon dioxide native substrate of carbonic anhydrase can also be reduced by a direct hydrogenation process. We have considered the following possible reaction mechanisms: (i) reductive elimination (two different paths in which a three- or five-centered transition state is possible); (ii) σ-bond metathesis and rotation of the formate; (iii) release of the formic acid product and the restoring of the catalytic cycle. In addition, for the reductive elimination, the possible mechanism that involves the assistance of a deep water molecule has also been explored. Our results show that

- In the first step of the reaction, the insertion and the activation of H_2 occur without an energy barrier.
- The subsequent insertion of carbon dioxide is possible with a relatively low energy requirement (6.9 kcal mol^{-1}).
- The favored reductive elimination path is that in which a five-centered transition state is formed. The required activation energy for this last process is 6.4 kcal mol^{-1}. Assistance by water can be excluded due to the high energetic barrier (11.4 kcal mol^{-1}).
- The σ-bond metathesis reaction mechanism is the favored path and all the minima and maxima intercepted on the potential energy surface lie below the asymptotic limit.
- The rate-determining step is that of restoring the catalytic cycle in which the formic acid product is released and the catalyst regenerated.

Our results indicate that this new modified Rh-carbonic anhydrase can act as a reductase also for the direct hydrogenation of carbon dioxide. We hope that our work can stimulate experimental studies to test this prediction.

ASSOCIATED CONTENT

Supporting Information

The Supporting Information is available free of charge on the ACS Publications website at DOI: 10.1021/acscatal.5b00185.

QM/QM′ and QM/MM computational details; comparison between QM cluster method, QM/QM′ and QM/MM ONIOM procedure **1a** species optimized structure; mechanism for the addition of H_2O to **1a** species; comparison between QM and QM/QM′ $\mathbf{TS_{1b+CO2-1c}}$ optimized structure; scan for searching of the five-membered ring $\mathbf{TS_{3a-3b}}$; intrinsic reaction-coordinate results for $\mathbf{TS_{1d-2a}}$, $\mathbf{TS_{4a-4b}}$, $\mathbf{TS_{5b-5c}}$, and $\mathbf{TS_{6a-6b}}$ transition states; pathway from **3b** species to the **6a** one (PDF)

Cartesian coordinates files of all the stationary points intercepted along the considered potential energy surfaces are separately given (ZIP)

AUTHOR INFORMATION

Corresponding Author

*E-mail: tmarino@unical.it.

DOI: 10.1021/acscatal.5b00185
ACS Catal. 2015, 5, 5397−5409

Author Contributions

The manuscript was written through contributions of all authors. All authors have given approval to the final version of the manuscript.

Notes

The authors declare no competing financial interest.

■ ACKNOWLEDGMENTS

This work was financially supported through the Department of Chemistry and Chemical Technologies of the Università della Calabria (Italy) and FP7- PEOPLE-2011-IRSES, Project no. 295172. P. Piazzetta gratefully acknowledges Commissione Europea, Fondo Sociale Europeo, and Regione Calabria for the financial support. D. R. Salahub is grateful to NSERC (Canada) for ongoing Discovery Grant support.

■ REFERENCES

(1) Suh, M. P.; Park, H. J.; Prasad, T. K.; Lim, D.-W. *Chem. Rev.* **2012**, *112*, 782−835.
(2) Coontz, R.; Hanson, B. *Science* **2004**, *305*, 957.
(3) Crabtree, G. W.; Dresselhaus, M. S.; Buchanan, M. V. *Phys. Today* **2004**, *57*, 39−44.
(4) U.S. DOE. Hydrogen, Fuel Cells & Infrastructure Technology Program (http://www.eere.energy.gov/hydrogenandfuelcells/storage).
(5) The American Physical Society. The Hydrogen Initiative (http://www.aps.org/public_affairs/index.cfm).
(6) Appel, A. M.; Bercaw, J. E.; Bocarsly, A. B.; Dobbek, H.; DuBois, D. L.; Dupuis, M.; Ferry, J. G.; Fujita, E.; Hille, R.; Kenis, P. J. A.; Kerfeld, C. A.; Morris, R. H.; Peden, C. H. F.; Portis, A. R.; Ragsdale, S. W.; Rauchfuss, T. B.; Reek, J. N. H.; Seefeldt, L. C.; Thauer, R. K.; Waldrop, G. L. *Chem. Rev.* **2013**, *113*, 6621−6658.
(7) Reda, T.; Plugge, C. M.; Abram, N. J.; Hirst, J. *Proc. Natl. Acad. Sci. U. S. A.* **2008**, *105*, 10654−10658.
(8) Aresta, M.; Dibenedetto, A. *Dalton Trans.* **2007**, 2975−2992.
(9) Benson, E. E.; Kubiak, C. P.; Sathrum, A. J.; Smieja, J. M. *Chem. Soc. Rev.* **2009**, *38*, 89−99.
(10) Finn, C.; Schnittger, S.; Yellowlees, L. J.; Love, J. B. *Chem. Commun.* **2012**, *48*, 1392−1399.
(11) Peters, M.; Köhler, B.; Kuckshinrichs, W.; Leitner, W.; Markewitz, P.; Müller, T. E. *ChemSusChem* **2011**, *4*, 1216−1240.
(12) Lewis, N. S.; Nocera, D. G. *Proc. Natl. Acad. Sci. U. S. A.* **2006**, *103*, 15729−15735.
(13) *Activation of Small Molecules: Organometallic and Bioinorganic Perspectives*; Tolman, W. B., Ed.; Wiley-VCH Verlag GmbH & Co. KGaA: Weinheim, Germany, 2006.
(14) Riduan, S. N.; Zhang, Y. *Dalton Trans.* **2010**, *39*, 3347−3357.
(15) Sakakura, T.; Choi, J.; Yasuda, H. *Chem. Rev.* **2007**, *107*, 2365−2387.
(16) Jessop, P. G.; Ikariya, T.; Noyori, R. *Chem. Rev.* **1995**, *95*, 259−272.
(17) Jessop, P. G.; Joo, F.; Tai, C. C. *Coord. Chem. Rev.* **2004**, *248*, 2425−2442.
(18) Leitner, W. *Angew. Chem., Int. Ed. Engl.* **1995**, *34*, 2207−2221.
(19) Wang, W.; Wang, S.; Ma, X.; Gong, J. *Chem. Soc. Rev.* **2011**, *40*, 3703−3727.
(20) Laurenczy, G. *Chimia* **2011**, *65*, 663−666.
(21) Boddien, A.; Mellmann, D.; Gartner, F.; Jackstell, R.; Junge, H.; Dyson, P. J.; Laurenczy, G.; Ludwig, R.; Beller, M. *Science* **2011**, *333*, 1733−1736.
(22) Johnson, T. C.; Morris, D. J.; Wills, M. *Chem. Soc. Rev.* **2010**, *39*, 81−88.
(23) Federsel, C.; Boddien, A.; Jackstell, R.; Jennerjahn, R.; Dyson, P. J.; Scopelliti, R.; Laurenczy, G.; Beller, M. *Angew. Chem., Int. Ed.* **2010**, *49*, 9777−9780.
(24) Langer, R.; Diskin-Posner, Y.; Leitus, G.; Shimon, L. J. W.; BenDavid, Y.; Milstein, D. *Angew. Chem., Int. Ed.* **2011**, *50*, 9948−9952.
(25) Jeletic, M. S.; Mock, M. T.; Appel, A. M.; Linehan, J. C. *J. Am. Chem. Soc.* **2013**, *135*, 11533−11536.
(26) Tai, C. C.; Chang, T.; Roller, B.; Jessop, P. G. *Inorg. Chem.* **2003**, *42*, 7340−7341.
(27) Annibale, V. T.; Song, D. *Organometallics* **2014**, *33*, 2776−2783.
(28) Hou, C.; Jiang, J.; Zhang, S.; Wang, G.; Zhang, Z.; Ke, Z.; Zhao, C. *ACS Catal.* **2014**, *4*, 2990−2997.
(29) Schuchmann, K.; Müller, V. *Science* **2013**, *342*, 1382−1385.
(30) Krishnamurthy, V. M.; Kaufman, G. K.; Urbach, A. R.; Gitlin, I.; Gudiksen, K. L.; Weibel, D. B.; Whitesides, G. M. *Chem. Rev.* **2008**, *108*, 946−1051.
(31) Baird, T. T., Jr.; Waheed, A.; Okuyama, T.; Sly, W. S.; Fierke, C. A. *Biochemistry* **1997**, *36*, 2669−2678.
(32) Hurt, J. D.; Tu, C.; Laipis, P. J.; Silverman, D. N. *J. Biol. Chem.* **1997**, *272*, 13512−13518.
(33) Earnhardt, J. N.; Qian, M.; Tu, C.; Lakkis, M. M.; Bergenhem, N. C. H.; Laipis, P. J.; Tashian, R. E.; Silverman, D. N. *Biochemistry* **1998**, *37*, 10837−10845.
(34) Lindskog, S.; Silverman, D. N. In *The Carbonic Anhydrases: New Horizons*; Chegwidden, W. R., Carter, N. D., Edwards, Y. H., Eds.; Birkhäuser Verlag: Basel, Switzerland, 2000; Vol. *90*.
(35) Chegwidden, W. R.; Carter, N. D. In *The Carbonic Anhydrases: New Horizons*; Chegwidden, W. R., Carter, N. D., Edwards, Y. H., Eds.; Birkhäuser Verlag: Basel, Switzerland, 2000; Vol. *90*.
(36) Lehtonen, J.; Shen, B.; Vihinen, M.; Casini, A.; Scozzafava, A.; Supuran, C. T.; Parkkila, A.-K.; Saarnio, J.; Kivelä, A. J.; Waheed, A.; Sly, W. S.; Parkkila, S. *J. Biol. Chem.* **2004**, *279*, 2719−2727.
(37) Nishimori, I.; Vullo, D.; Innocenti, A.; Scozzafava, A.; Mastrolorenzo, A.; Supuran, C. T. *J. Med. Chem.* **2005**, *48*, 7860−7866.
(38) Nishimori, I.; Minakuchi, T.; Onishi, S.; Vullo, D.; Scozzafava, A.; Supuran, C. T. *J. Med. Chem.* **2007**, *50*, 381−388.
(39) Nishimori, I.; Vullo, D.; Innocenti, A.; Scozzafava, A.; Mastrolorenzo, A.; Supuran, C. T. *Bioorg. Med. Chem. Lett.* **2005**, *15*, 3828−3833.
(40) Jing, Q.; Okrasa, K.; Kazlauskas, R. J. *Chem. - Eur. J.* **2009**, *15*, 1370−1376.
(41) Jing, Q.; Kazlauskas, R. J. *ChemCatChem* **2010**, *2*, 953−957.
(42) Musashi, Y.; Sakaki, S. *J. Am. Chem. Soc.* **2002**, *124*, 7588−7603.
(43) Aresta, M.; Dibenedetto, A.; Angelini, A. *Chem. Rev.* **2014**, *114*, 1709−1742.
(44) Piazzetta, P.; Marino, T.; Russo, N. *Inorg. Chem.* **2014**, *53*, 3488−3493.
(45) Piazzetta, P.; Marino, T.; Russo, N. *Phys. Chem. Chem. Phys.* **2014**, *16*, 16671−16676.
(46) Becke, A. D. J. *J. Chem. Phys.* **1993**, *98*, 5648−5652.
(47) Lee, C. T.; Yang, W. T.; Parr, R. G. *Phys. Rev. B: Condens. Matter Mater. Phys.* **1988**, *37*, 785−789.
(48) Frisch, M. J.; Trucks, G. W.; Schlegel, H. B.; Scuseria, G. E.; Robb, M. A.; Cheeseman, J. R.; Montgomery, Jr., J. A.; Vreven, T.; Kudin, K. N.; Burant, J. C.; Millam, J. M.; Iyengar, S. S.; Tomasi, J.; Barone, V.; Mennucci, B.; Cossi, M.; Scalmani, G.; Rega, N.; Petersson, G. A.; Nakatsuji, H.; Hada, M.; Ehara, M.; Toyota, K.; Fukuda, R.; Hasegawa, J.; Ishida, M.; Nakajima, T.; Honda, Y.; Kitao, O.; Nakai, H.; Klene, M.; Li, X.; Knox, J. E.; Hratchian, H. P.; Cross, J. B.; Bakken, V.; Adamo, C.; Jaramillo, J.; Gomperts, R.; Stratmann, R. E.; Yazyev, O.; Austin, A. J.; Cammi, R.; Pomelli, C.; Ochterski, J. W.; Ayala, P. Y.; Morokuma, K.; Voth, G. A.; Salvador, P.; Dannenberg, J. J.; Zakrzewski, V. G.; Dapprich, S.; Daniels, A. D.; Strain, M. C.; Farkas, O.; Malick, D. K.; Rabuck, A. D.; Raghavachari, K.; Foresman, J. B.; Ortiz, J. V.; Cui, Q.; Baboul, A. G.; Clifford, S.; Cioslowski, J.; Stefanov, B. B.; Liu, G.; Liashenko, A.; Piskorz, P.; Komaromi, I.; Martin, R. L.; Fox, D. J.; Keith, T.; Al-Laham, M. A.; Peng, C. Y.; Nanayakkara, A.; Challacombe, M.; Gill, P. M. W.; Johnson, B.; Chen, W.; Wong, M. W.; Gonzalez, C.; Pople, J. A.; *Gaussian 03*, Revision C.02; Gaussian, Inc.: Wallingford, CT, 2004.

DOI: 10.1021/acscatal.5b00185
ACS Catal. 2015, 5, 5397−5409

(49) Andrae, D.; Haussermann, U.; Dolg, M.; Stoll, H.; Preuss, H. *Theor. Chim. Acta* **1990**, *77*, 123−141.
(50) Barone, V.; Cossi, M. *J. Phys. Chem. A* **1998**, *102*, 1995−2001.
(51) Cossi, M.; Rega, N.; Scalmani, G.; Barone, V. *J. Comput. Chem.* **2003**, *24*, 669−681.
(52) Grimme, S.; Antony, J.; Ehrlich, S.; Krieg, H. *J. Chem. Phys.* **2010**, *132*, (154104)-1−(154104)-19.
(53) Grimme, S.; Ehrlich, S.; Goerigk, L. *J. Comput. Chem.* **2011**, *32*, 1456−1465.
(54) Siegbahn, P. E. M; Blomberg, M. R. A. *Chem. Rev.* **2000**, *100*, 421−437.
(55) Warshel, A. *Computer Modeling of Chemical Reactions in Enzymes and Solutions*; Wiley: New York, 1991.
(56) Ramos, M. J.; Fernandes, P. A. *Acc. Chem. Res.* **2008**, *41* (6), 689−698.
(57) Blomberg, M. R. A.; Borowski, T.; Himo, F.; Liao, R.-Z.; Siegbahn, P. E. M. *Chem. Rev.* **2014**, *114*, 3601−3658.
(58) Siegbahn, P. E. M.; Himo, F. *JBIC, J. Biol. Inorg. Chem.* **2009**, *14*, 643−651.
(59) Siegbahn, P. E. M.; Himo, F. *Wiley Interdiscip. Rev.: Comput. Mol. Sci.* **2011**, *1*, 323−336.
(60) Fukui, K. *J. Phys. Chem.* **1970**, *74*, 4161−4163.
(61) Gonzalez, C.; Schlegel, H. B. *J. Chem. Phys.* **1989**, *90*, 2154−2161.
(62) Glendening, E. D.; Reed, A. E.; Carpenter, J. E.; Weinhold, F. *NBO*, version 3.1.
(63) Marino, T.; Russo, N.; Toscano, M. *J. Am. Chem. Soc.* **2005**, *127*, 4242−4253.
(64) Bottoni, A.; Lanza, C. Z.; Miscione, G. P.; Spinelli, D. *J. Am. Chem. Soc.* **2004**, *126*, 1542−1550.
(65) Miscione, G. P.; Stenta, M.; Spinelli, D.; Anders, E.; Bottoni, A. *Theor. Chem. Acc.* **2007**, *118*, 193−201.
(66) Rossi, A.; Hoffmann, R. *Inorg. Chem.* **1975**, *14*, 365−374.
(67) Siegbahn, P. E. M; Blomberg, M. R. A. In *Theoretical Aspects of Homogeneous Catalysis*; van Leeuwen, P. W. N. M., Morokuma, K., van Lenthe, J. H., Eds.; Kluwer Academic Publishers: Dordrecht, 1995.
(68) Musashi, Y.; Sakaki, S. *J. Chem. Soc., Dalton Trans.* **1998**, 577−584.
(69) Braunstein, P.; Matt, D.; Nobel, D. *Chem. Rev.* **1988**, *88*, 747−764.
(70) Mellot-Draznieks, C.; Valayannopoulos, V.; Chrétien, D.; Munnich, A.; de Lonlay, P.; Toulhoat, H. *ACS Catal.* **2012**, *2* (12), 2673−2686.
(71) Jackson, C. J.; Foo, J.-L.; Tokuriki, N.; Afriat, L.; Carr, P. D.; Kim, H.-K.; Schenk, G.; Tawfik, D. S.; Ollis, D. L. *Proc. Natl. Acad. Sci. U. S. A.* **2009**, *106*, 21631−21636.
(72) Hutschka, F.; Dedieu, A.; Eichberger, M.; Fornika, R.; Leitner, W. *J. Am. Chem. Soc.* **1997**, *119*, 4432−4443.
(73) Jessop, P. G.; Hsiao, Y.; Ikariya, T.; Noyori, R. *J. Am. Chem. Soc.* **1996**, *118*, 344−355.

DOI: 10.1021/acscatal.5b00185
ACS Catal. 2015, 5, 5397−5409